Rogue wave generation by inelastic quasi-soliton collisions in optical fibres

M. EBERHARD,[1] A. SAVOJARDO,[2,*] A. MARUTA,[3] AND R. A. RÖMER[2]

[1] *Electrical, Electronic and Power Engineering, School of Engineering and Applied Science, Aston University, Aston Triangle, Birmingham B4 7ET, UK*
[2] *Department of Physics and Centre for Scientific Computing, The University of Warwick, Coventry CV4 7AL, UK*
[3] *Division of Electrical, Electronic and Information Engineering, Graduate School of Engineering, Osaka University, Suita Campus, Japan*
[*] *a.savojardo@warwick.ac.uk*

Abstract: Optical "rogue" waves are rare and very high intensity pulses of light that occur in optical devices such as communication fibers. They appear suddenly and can cause transmission errors and damage in optical communication systems. Indeed, the physics governing their dynamics is very similar to "monster" or "freak" waves on the Earth's oceans, which are known to harm shipping. It is therefore important to characterize rogue wave generation, dynamics and, if possible, predictability. Here we demonstrate a simple cascade mechanism that drives the formation and emergence of rogue waves in the generalized non-linear Schrödinger equation with third-order dispersion. This generation mechanism is based on *inelastic collisions* of quasi-solitons and is well described by a resonant-like scattering behaviour for the energy transfer in pair-wise quasi-soliton collisions. Our theoretical and numerical results demonstrate a threshold for rogue wave emergence and the existence of a period of reduced amplitudes — a "calm before the storm" — preceding the arrival of a rogue wave event. Comparing with ultra-long time window simulations of 3.865×10^6ps we observe the statistics of rogue waves in optical fibres with an unprecedented level of detail and accuracy, unambiguously establishing the long-ranged character of the rogue wave power-distribution function over seven orders of magnitude.

References and links

1. L. Draper, "'Freak' ocean waves," Oceanus **10**, 13–15 (1964).
2. L. Draper, "Severe wave conditions at sea," J. Inst. Navig. **24**, 273–277 (1971).
3. J. Mallory, "Abnormal waves in the south-east coast of South Africa," Int. Hydrog. Rev. **51**, 89–129 (1974).
4. S. Perkins, "Dashing Rogues," Sci. News **170**, 328 (2006).
5. M. Erkintalo, "Rogue waves: Predicting the unpredictable?" Nat. Photonics **9**, 560–562 (2015).
6. M. Hopkin, "Sea snapshots will map frequency of freak waves," Nature **430**, 492 (2004).
7. C. Kharif and E. Pelinovsky, "Physical mechanisms of the rogue wave phenomenon," Eur. J. Mech. B/Fluids **22**, 603 – 634 (2003).
8. M. Onorato, A. R. Osborne, M. Serio, L. Cavaleri, C. Brandini, and C. T. Stansberg, "Observation of strongly non-Gaussian statistics for random sea surface gravity waves in wave flume experiments," Phys. Rev. E **70**, 067302 (2004).
9. T. A. A. Adcock, P. H. Taylor, and S. Draper, "Nonlinear dynamics of wave-groups in random seas: unexpected walls of water in the open ocean," Proc. Roy. Soc. A: Math. Phys. Eng. Sci. **471**, 20150660 (2015).
10. M. Onorato, S. Residori, U. Bortolozzo, A. Montina, and F. Arecchi, "Rogue waves and their generating mechanisms in different physical contexts," Phys. Rep. **528**, 47–89 (2013).
11. J. M. Dudley, F. Dias, M. Erkintalo, and G. Genty, "Instabilities, breathers and rogue waves in optics," Nature **8**, 755–764 (2014).
12. A. Chabchoub, N. Hoffmann, M. Onorato, G. Genty, J. M. Dudley, and N. Akhmediev, "Hydrodynamic supercontinuum," Phys. Rev. Lett. **111**, 054104 (2013).

13. D. R. Solli, C. Ropers, P. Koonath, and B. Jalali, "Optical rogue waves," Nature **450**, 1054–1057 (2007).
14. D. R. Solli, C. Ropers, and B. Jalali, "Active control of rogue waves for stimulated supercontinuum generation," Phys. Rev. Lett. **101**, 233902 (2008).
15. M. Erkintalo, G. Genty, and J. M. Dudley, "Rogue-wave-like characteristics in femtosecond supercontinuum generation," Opt. Lett. **34**, 2468 (2009).
16. B. Kibler, C. Finot, and J. M. Dudley, "Soliton and rogue wave statistics in supercontinuum generation in photonic crystal fibre with two zero dispersion wavelengths," Eur. Phys. J. Spec. Top. **173**, 289–295 (2009).
17. S. Randoux, P. Walczak, M. Onorato, and P. Suret, "Intermittency in integrable turbulence," Phys. Rev. Lett. **113**, 113902 (2014).
18. P. Walczak, S. Randoux, and P. Suret, "Optical rogue waves in integrable turbulence," Phys. Rev. Lett. **114**, 143903 (2015).
19. S. Birkholz, C. Brée, A. Demircan, and G. Steinmeyer, "Predictability of Rogue Events," Phys. Rev. Lett. **114**, 213901 (2015).
20. J. Kasparian, P. Béjot, J.-P. Wolf, and J. M. Dudley, "Optical rogue wave statistics in laser filamentation," Opt. Express **17**, 12070 (2009).
21. A. Montina, U. Bortolozzo, S. Residori, and F. T. Arecchi, "Non-Gaussian statistics and extreme waves in a nonlinear optical cavity," Phys. Rev. Lett. **103**, 173901 (2009).
22. C. Bonatto, M. Feyereisen, S. Barland, M. Giudici, C. Masoller, J. R. R. Leite, and J. R. Tredicce, "Deterministic optical rogue waves," Phys. Rev. Lett. **107**, 053901 (2011).
23. C. Lecaplain, P. Grelu, J. M. Soto-Crespo, and N. Akhmediev, "Dissipative rogue waves generated by chaotic pulse bunching in a mode-locked laser," Phys. Rev. Lett. **108**, 233901 (2012).
24. S. Randoux and P. Suret, "Experimental evidence of extreme value statistics in Raman fiber lasers," Opt. Lett. **37**, 500–502 (2012).
25. K. Hammani, C. Finot, J. M. Dudley, and G. Millot, "Optical rogue-wave-like extreme value fluctuations in fiber Raman amplifiers," Opt. Express **16**, 16467 (2008).
26. N. Akhmediev and E. Pelinovsky, "Editorial – Introductory remarks on "Discussion & Debate: Rogue Waves – Towards a Unifying Concept?"" Eur. Phys. J. Spec. Top. **185**, 1–4 (2010).
27. V. Ruban, Y. Kodama, M. Ruderman, J. Dudley, R. Grimshaw, P. V. E. McClintock, M. Onorato, C. Kharif, E. Pelinovsky, T. Soomere, G. Lindgren, N. Akhmediev, A. Slunyaev, D. Solli, C. Ropers, B. Jalali, F. Dias, and A. Osborne, "Rogue waves–towards a unifying concept: discussions and debates," Eur. Phys. J. Spec. Top. **185**, 5–15 (2010).
28. N. Akhmediev, B. Kibler, F. Baronio, M. Belić, W.-P. Zhong, Y. Zhang, W. Chang, J. M. Soto-Crespo, P. Vouzas, P. Grelu, C. Lecaplain, K. Hammani, S. Rica, A. Picozzi, M. Tlidi, K. Panajotov, A. Mussot, A. Bendahmane, P. Szriftgiser, G. Genty, J. Dudley, A. Kudlinski, A. Demircan, U. Morgner, S. Amiraranashvili, C. Bree, G. Steinmeyer, C. Masoller, N. G. R. Broderick, A. F. J. Runge, M. Erkintalo, S. Residori, U. Bortolozzo, F. T. Arecchi, S. Wabnitz, C. G. Tiofack, S. Coulibaly, and M. Taki, "Roadmap on optical rogue waves and extreme events," J. Opt. **18**, 063001 (2016).
29. B. Kibler, J. Fatome, C. Finot, G. Millot, F. Dias, G. Genty, N. Akhmediev, and J. M. Dudley, "The Peregrine soliton in nonlinear fibre optics," Nat. Phys. **6**, 790–795 (2010).
30. A. Chabchoub, N. P. Hoffmann, and N. Akhmediev, "Rogue wave observation in a water wave tank," Phys. Rev. Lett. **106**, 204502 (2011).
31. B. Kibler, J. Fatome, C. Finot, G. Millot, G. Wetzel, N. Akhmediev, F. Dias, and J. M. Dudley, "Observation of Kuznetsov-Ma soliton dynamics in optical fibre," Sci. Rep. **2**, 463 (2012).
32. M. Onorato, A. R. Osborne, M. Serio, and L. Cavaleri, "Modulational instability and non-Gaussian statistics in experimental random water-wave trains," Phys. Flu. **17**, 078101 (2005).
33. R. Höhmann, U. Kuhl, H.-J. Stöckmann, L. Kaplan, and E. J. Heller, "Freak waves in the linear regime: A microwave study," Phys. Rev. Lett. **104**, 093901 (2010).
34. N. Akhmediev, J. M. Soto-Crespo, and A. Ankiewicz, "Could rogue waves be used as efficient weapons against enemy ships?" Eur. Phys. J. Spec. Top. **185**, 259–266 (2010).
35. G. Weerasekara, A. Tokunaga, H. Terauchi, M. Eberhard, and A. Maruta, "Soliton's eigenvalue based analysis on the generation mechanism of rogue wave phenomenon in optical fibers exhibiting weak third order dispersion," Opt. Express **23**, 143 (2015).
36. F. Luan, D. V. Skryabin, A. V. Yulin, and J. C. Knight, "Energy exchange between colliding solitons in photonic crystal fibers," Opt. Express **14**, 9844 (2006).
37. A. Mussot, A. Kudlinski, M. Kolobov, E. Louvergneaux, M. Douay, and M. Taki, "Observation of extreme temporal events in CW-pumped supercontinuum," Opt. Express **17**, 17010–17015 (2009).
38. A. Armaroli, C. Conti, and F. Biancalana, "Rogue solitons in optical fibers: a dynamical process in a complex energy landscape?" Optica **2**, 497 (2015).
39. C. Brée, G. Steinmeyer, I. Babushkin, U. Morgner, and A. Demircan, "Controlling formation and suppression of fiber-optical rogue waves," Opt. Lett. **41**, 3515 (2016).
40. A. Demircan, S. Amiranashvili, C. Br?e, C. Mahnke, F. Mitschke, and G. Steinmeyer, "Rogue wave formation by accelerated solitons at an optical event horizon," Appl. Phys. B **115**, 343–354 (2014).
41. G. Genty, C. de Sterke, O. Bang, F. Dias, N. Akhmediev, and J. Dudley, "Collisions and turbulence in optical rogue

wave formation," Phys. Lett. A **374**, 989–996 (2010).

42. V. V. Voronovich, V. I. Shrira, and G. Thomas, "Can bottom friction suppress 'freak wave' formation?" J. Flu. Mech. **604**, 263–296 (2008).

43. V. Zakharov, A. Pushkarev, V. Shvets, and V. Yan'kov, "Soliton turbulence," Pis'ma v Zhurnal Eksperimental'noi i Teoreticheskoi Fiziki **48**, 79–82 (1988).

44. U. Bortolozzo, J. Laurie, S. Nazarenko, and S. Residori, "Optical wave turbulence and the condensation of light," J. Opt. Soc. Am. B **26**, 2280 (2009).

45. A. Picozzi, J. Garnier, T. Hansson, P. Suret, S. Randoux, G. Millot, and D. Christodoulides, "Optical wave turbulence," Phys. Rep. **542**, 1–132 (2014).

46. M. Eberhard, "Massively parallel optical communication system simulator," https://github.com/Marc-Eberhard/MPOCSS.

47. G. P. Agrawal, *Nonlinear Fiber Optics* (Academic Press, 2013).

48. V. E. Zakharov and A. B. Shabat, "Exact theory of two-dimensional self-focusing and one dimensional self-modulation of waves in nonlinear media," Sov. Phys. JETP **34**, 62–69 (1972).

49. V. E. Zakharov, "Turbulence in Integrable Systems," Stud. Appl. Math. **122**, 219–234 (2009).

50. M. Taki, A. Mussot, A. Kudlinski, E. Louvergneaux, M. Kolobov, and M. Douay, "Third-order dispersion for generating optical rogue solitons," Phys. Lett. A **374**, 691–695 (2010).

51. N. Akhmediev and M. Karlsson, "Cherenkov radiation emitted by solitons in optical fibers," Phys. Rev. A **51**, 2602–2607 (1995).

52. K. Tai, A. Hasegawa, and A. Tomita, "Observation of modulational instability in optical fibers," Phys. Rev. Lett. **56**, 135–138 (1986).

53. A. Hasegawa, "Generation of a train of soliton pulses by induced modulational instability in optical fibers," Opt. Lett. **9**, 288 (1984).

54. V. Karpman and V. Solov'ev, "A perturbational approach to the two-soliton systems," Phys. D: Nonlin. Phenom. **3**, 487–502 (1981).

55. A. V. Buryak and N. N. Akhmediev, "Internal friction between solitons in near-integrable systems," Phys. Rev. E **50**, 3126–3133 (1994).

56. H. Degueldre, J. M. Jakob, T. Geisel, and R. Fleischmann, "Random focusing of tsunami waves," Nat. Phys. **12**, 259–262 (2016).

57. A. Slunyaev and E. Pelinovsky, "Role of Multiple Soliton Interactions in the Generation of Rogue Waves: The Modified Korteweg-de Vries Framework," Phys. Rev. Lett. **117**, 214501 (2016).

58. Y.-H. Sun, "Soliton synchronization in the focusing nonlinear Schrödinger equation," Phys. Rev. E **93**, 052222 (2016).

59. M. Eberhard, A. Savojardo, A. Maruta, and R. A. Römer, "Rogue wave generation by inelastic quasi-soliton collisions in optical fibres," http://dx.doi.org/10.17036/5067df69-bf43-4bea-a5ff-f0792001d573 (2017).

60. W. H. Press, B. P. Flannery, S. A. Teukolsky, and W. T. Vetterling, *Numerical Recipes in C*, 2nd ed. (Cambridge University, 1992).

61. Y. Nagashima, *Elementary Particle Physics*, vol. 1, (Wiley-Vch,2010).

62. Z. Chen, A. J. Taylor, and A. Efimov, "Soliton dynamics in non-uniform fiber tapers: analytical description through an improved moment method," J. Opt. Soc. Am. B **27**, 1022 (2010).

63. J. Santhanam and G. P. Agrawal, "Raman-induced spectral shifts in optical fibers: general theory based on the moment method," Opt. Commun. **222**, 413–420 (2003).

64. A. Savojardo, "Rare events in optical fibers", PhD Thesis (2017).

1. Introduction

Historically, reports of "monster" or "freak" waves [1–3] on the earth's oceans have been seen largely as sea men's tales [4, 5]. However, the recent availability of reliable experimental observations [4, 6] has proved their existence and shown that these "rogues" are indeed rare events [7], governed by long tails in their probability distribution function (PDF) [8], and hence concurrent with very large wave amplitudes [9, 10]. As both deep water waves in the oceans and optical waves in fibres can be described by similar generalized non-linear Schrödinger equations (gNLSE) they both show rogue waves (RW) and long-tail statistics [8, 11, 12]. The case of RW generation in optical fibres during super-continuum generation has been observed experimentally [13–16]. Recently, experimental data of long tails in the PDF have been collected [17, 18], as well as time correlations in various wave phenomena with RW occurrence studied [19]. RWs and long-tailed PDFs have also been found during high power femtosecond pulse filamentation in air [20], in non-linear optical cavities [21] and in the output intensity of optically injected semiconductors laser [22], mode-locked fiber lasers [23], Raman fiber lasers [24] and fiber Raman amplifiers [25]. However, it still remains largely unknown how RWs

emerge [26–28] and theoretical explanations range from high-lighting the importance of the non-linearity [9, 29–31] to those based on short-lived linear superpositions of quasi-solitons during collisions [32, 33].

Here we will show that there is also a process to generate rogue waves through an *energy-exchange mechanism* when collisions become *inelastic* in the presence of a third-order dispersion (TOD) term [34, 35]. Energy-exchange in NLSEs has indeed been observed experimentally [36, 37] and numerically [38–41] although no quantitative description of the process has been given. Recent studies confirmed experimentally and numerically that the presence of TOD in optical fibers turns the system convectively unstable and generates extraordinary optical intensities [7, 42]. Energy exchange mechanisms have also been observed in the context of optical waves turbulence [43–45]. We derive a *cascade model* that simulates the RW generation process directly without the need for a full numerical integration of the gNLSE. The model is validated using a massively parallel simulation [46], allowing us to achieve an unprecedented level of detail through the concurrent use of tens of thousands of CPU cores. Based on statistics from more than 17×10^6 interacting quasi-solitons, find that the results of the full gNLSE integration and the cascade model exhibit the same quantitative, long-tail PDF. This agreement highlights the importance of (i) a resonance-like two-soliton scattering coupled with (ii) quasi-soliton energy exchange in giving rise to RWs. We furthermore find that the cascade model and the full gNLSE integration exhibit a "calm-before-the-storm" effect of reduced amplitudes prior to the arrival of the RW, hence hinting towards the possibility of RW prediction. Last, we demonstrate that there is a sharp threshold for TOD to be strong enough to lead to the emergence of RWs.

2. Rogue waves as cascades of interacting solitons

Analytical soliton solutions for the generalized non-linear Schrödinger equation

$$\partial_z u + \frac{i\beta_2}{2} \partial_t^2 u - \frac{\beta_3}{6} \partial_t^3 u - i\gamma |u|^2 u = 0 \tag{1}$$

are only known for $\beta_3 = 0$. Here $u(z, t)$ describes a slowly varying pulse envelope, γ the non-linear coefficient, β_2 (< 0) the normal group velocity dispersion and β_3 the TOD [47]. We shall, due to the relatively short distances of only a few kilometers in a super-continuum experiment, neglect the effects of absorption and the shock term [11]; we find that the effects of the delayed Raman response are similar to TOD and will be commented at the end. Our aim hence is not the most accurate microscopic description possible, but the most simplistic numerical model that is still capable of generating RWs.

Without TOD β_3, the model (1) can be solved analytically and a $u(z, t)$ describing the celebrated *soliton* solutions can be found [48]. Depending on the phase difference between two such solitons, attracting or repulsing forces exist between them. This then leads to them either moving through each other unchanged or swapping their positions. The solitons emerge unchanged with the same energy as they had before the collision. This type of collision is elastic and it is the only known type of collision for true analytic (integrable) solitons [26, 49]. When we introduce β_3, the system can no longer be solved analytically and no closed-form solutions are known in general. Numerical integration of Eq. (1) shows that stable pulses still exist and these propagate individually much like solitons in the $\beta_3 = 0$ case [50]. These *quasi-solitons*, and collisions between them, are in many cases as elastic as they are for integrable solitons. However, when two quasi-solitons have a matching phase, energy can be transferred between them leading to one gaining and the other losing energy [34]. In addition, the emerging pulses have to shed energy through dispersive waves until they have relaxed back to a stable quasi-soliton state [51].

Based on this observation we can now replace the full numerical integration of the gNLSE with a *phenomenological cascade model* that tracks the collisions between quasi-solitons. Our starting point are quasi-solitons with exponential power tails as found in a super-continuum

system after the modulation instability has broken up the initial CW pump laser input into a train of pulses [47, 52, 53]. We generate a list of such quasi-solitons as our initial condition by randomly choosing the power levels P_q, phases ϕ_q and frequency shifts Ω_q in accordance with the statistics found in a real system at that point of the integration. The shape of a quasi-soliton is approximated by

$$u_q(z,t) = \sqrt{P_q} \, \text{sech}\left[\frac{(t-t_q) + z/v_q}{T_q}\right] \exp\left[i\phi_q\right] \qquad (2)$$

with effective period

$$T_q = \sqrt{\frac{|\beta_2 + \beta_3 \Omega_q|}{\gamma P_q}} \qquad (3)$$

and inverse velocity

$$v_q^{-1} = \beta_2 \Omega_q + \frac{\beta_3}{2} \Omega_q^2 + \frac{\beta_3}{6T_q^2} \qquad (4)$$

for each quasi-soliton labelled by q. Note that due to Eq. (3), the velocity v_q of a quasi-soliton depends on its power in addition to the frequency shift for $\beta_3 \neq 0$. We calculate which quasi-solitons will collide first, based on their known initial times t_q and velocities v_q. The phase difference $\phi_q - \phi_p$ between two quasi-solitons is drawn randomly from a uniform distribution in the interval $[0, 2\pi[$. Then we calculate the energy transferred from the smaller quasi-soliton to the larger via

$$\frac{\Delta E_1}{E_2} = \frac{\epsilon_{\text{eff}}}{|v_1^{-1} - v_2^{-1}|} \sin^2\left(\frac{\phi_1 - \phi_2}{2}\right), \qquad (5)$$

where ΔE_1 is the energy gain for the higher energy quasi-soliton and E_2 is the energy of the second quasi-soliton involved in the collision. A detailed justification of Eq. (5) and a discussion of the cross-section coefficient ϵ_{eff} will be given in the appendix. At this point we estimate the next collision to occur from the set of updated v_q and continue as described above until the simulation has reached the desired distance z. Obviously, this procedure is much simpler than a numerical integration of the gNLSE (1). The main strength of the model is a new qualitative and quantitative understanding of RW emergence and dynamics.

3. Rare events with ultra-long tails in the PDF

To compare the results with the full numerical integration we generate a power-distribution function (PDF) of the power levels at fixed distances Δz from $u(z,t) = \sum_q u_q(z,t)$ using the full quasi-soliton waveform (2). The PDF for the complete set of $\gtrsim 17 \times 10^6$ pulses propagating over 1500m is shown in Fig. 1(a) and 1(b) for selected distances for cascade model and gNLSE, respectively, using, for the gNLSE, a highly-optimised, massively parallel and linearly-scaling numerical procedure [46]. After 100m, the PDF exhibits a roughly exponential distribution as seen in Fig. 1(a). With $\beta_3 = 0$ this exponential PDF remains stable from this point onwards (cp. inset). However, with $\beta_3 \neq 0$ the inelastic collision of the quasi-solitons leads to an ever increasing number of high-energy RWs. After 500m, a clear deviation from the exponential distribution of the $\beta_3 = 0$ case has emerged and beyond 1000m, the characteristic L-shape of a fully-developed RW PDF has formed. The PDFs for both gNLSE and the cascade model in Figs. 1(a) and 1(b) then continue to evolve towards higher peak powers with some quasi-solitons becoming larger and larger. We remark that while fits descriptions of the PDF with Weibull, Pareto and stretched exponential are possible, no such fit is convincing across the full range 0-1000 W (see Figs. 1 (a) and 1(b) and Appendix C). In the inset of Fig. 1(b), we compare the long tail behaviour of both PDFs directly. We see that the agreement for PDFs is excellent taking into account that we have reduced the full integration of the gNLSE to only discrete collision
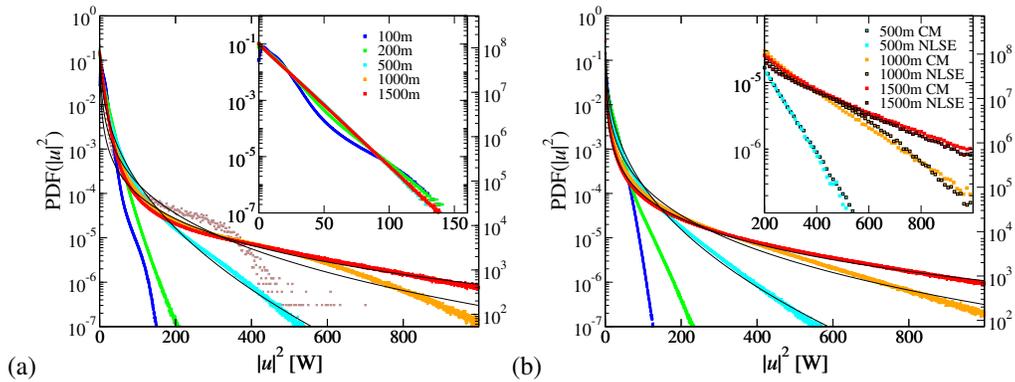
Fig. 1. (a) PDFs of the intensity $|u|^2$ from the gNLSE (1) at $\beta_3 = 2.64 \times 10^{-42}\text{s}^3\text{m}^{-1}$ using a large time window of $\Delta t = 3.865 \times 10^6\text{ps}$. The PDFs have been computed at distances $z = 100\text{m}, 200\text{m}, 500\text{m}, 1000\text{m}$ and 1500m. The left vertical axis denotes the values of the normalized PDF while the right vertical axis gives the event count per bin. The PDFs have been fitted using the Weibull function (full black lines). The brown points represnt the PDF calculate for a small time window of 200ps at 1500m. The inset shows results for $\beta_3 = 0$. (b) PDFs of the intensity $|u|^2$ from the cascade model for the same distances as in (a), using the same symbol and axes conventions. The PDFs have been fitted using the Weibull function (full black lines). The inset shows a comparison between the results from the gNLSE (colored lines) and the cascade model (black lines and symbol outlines) for $z = 500\text{m}, 1000\text{m}$ and 1500m. Only every 50th symbol is shown.

events between quasi-solitons. Thus, we find that the essence of the emergence of RWs in this system is very well captured by a process due to inelastic collisions.

4. Mechanisms of the cascade

In Fig. 2, we show a representative example for the propagation of $u(z,t)$, in the full gNLSE and the cascade model, in a short 15ps time range out of the full 3.865×10^6 ps with $\beta_2 = -2.6 \times 10^{-28}\text{s}^2\text{m}^{-1}$ and $\gamma = 0.01 \text{ W}^{-1}\text{m}^{-1}$. A small initial noise leads to differences in the pulse powers and velocities and hence to eventual collisions of neighbouring pulses. In the enlarged trajectory plots Figs. 2(b) and 2(c), we see that for $\beta_3 = 0$ the solitons interact elastically and propagate on average with the group velocity of the frame. However, for finite β_3 in Fig. 2(c), most collisions are *inelastic* and one quasi-soliton, with higher energy, moves through the frame from left to right due to its higher energy and group velocity mismatch compared to the frame. It collides in rapid succession with the other quasi-solitons travelling, on average, at the frame velocity. From Fig. 2(b), we see that our cascade model, in which we have replaced the intricate dynamics of the collission by an effective process, similarly shows quasi-solitons starting to collide inelastically, some emerging with higher energies and exhibiting a reduced group velocity. Note that in the cascade model we use an initial pulse power distribution that mimics the PDF of the gNLSE at 100m, and thus only generate data from 100m onwards (cp. appendix).

The main ingredient of the cascade model, the energy exchange, is obvious in the gNLSE results: in almost all cases, energy is transferred from the quasi-soliton with less energy to the one with more energy leading to the cascade of incremental gains for the more powerful quasi-soliton. This pattern is visible throughout Fig. 2(a) where initial differences in energy of quasi-solitons become exacerbated over time and larger and larger quasi-solitons emerge. These accumulate the energy of the smaller ones to the point that the smaller ones eventually vanish into the background. In addition, the group velocity of a quasi-soliton with TOD is dependent on
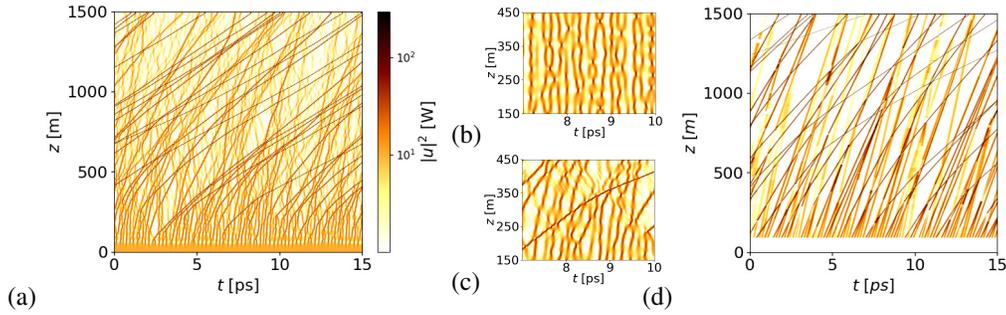
Fig. 2. (a) Intensity $|u(z,t)|^2$ for $\beta_3 = 2.64 \times 10^{-42} \mathrm{s}^3 \mathrm{m}^{-1}$ of the gNLSE Eq. (1) as function of the time t and distance z in a selected time frame of $\Delta t = 15$ps and distance range $\Delta z = 1.5$km. (b) $|u|^2$ with $\beta_3 = 0$ for a zoomed-in distance and time region, (c) $|u|^2$ with β_3 value as in (a) for a region of (a) with Δt and Δz chosen identical to (b). (d) Intensities $|u|^2$ as computed from the effective cascade model using the same shading/color scale as in (a). Note that we start the effective model at $z_0 = 100$m to mimic the effects of the modulation instability in (a).
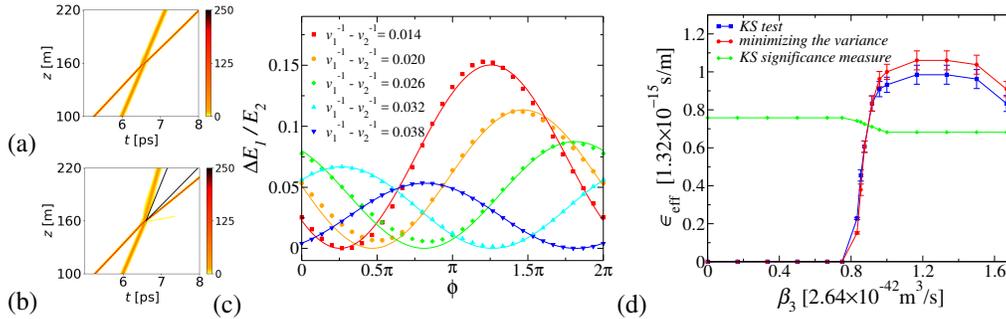
Fig. 3. (a+b) Intensities $|u(z,t)|^2$ of the scattering between two quasi-solitons. The phase difference ϕ was chosen to correspond to (a) the minimum and (b) the maximum of $\Delta E_1/E_2(\phi)$. (c) $\Delta E_1/E_2(\phi)$ for various choices of initial speeds. The data points represents results of the gNLSE (1) while the lines denote the fit (5). (d) ϵ values have been obtained comparing the PDF from the gNLSE and the cascade model at short distance using a Kolmogorov-Smirnov-like (KS) test and minimizing the variance (cf. appendix B). A KS significance measure is also shown [60].

the power of the quasi-soliton [47]. Thus, the emerging powerful quasi-solitons feature a growing group velocity difference to their peers and this increases their collision rate leading to even stronger growth. This can clearly be seen from Fig. 2(a) where larger-energy quasi-solitons start to move sideways as their velocity no longer matches the group velocity of the frame after they have acquired energy from other quasi-solitons due to inelastic collisions. Indeed, the relatively few remaining, soliton-like pulses at 1500m can have peak powers exceeding 1000W. They are truly self-sustaining rogues that have increased their power values by successive interactions and energy exchange with less powerful pulses.

5.   A threshold for RW emergence

We find that the emergence of RW behaviour relies on the presence of "enough" $\beta_3 \neq 0$ TOD — or similar additional terms in Eq. (1). Even then, the conditions for the cascade to start are subtle as we show in Fig. 3 for two quasi-soliton collisions with $\beta_3 = 2.64 \times 10^{-42} \mathrm{s}^3 \mathrm{m}^{-1}$.

The initial conditions for both collisions have been chosen to be identical apart from the relative phase between the two quasi-solitons: an earlier quasi-soliton with initially large power (200W) is met by a later, initially weak pulse (50W). Clearly, the collision of these two quasi-solitons as shown in Fig. 3(a) is (nearly) elastic, they simply exchange their positions, while retaining their individual power. This situation retains much of the dynamics from the $\beta_3 = 0$ case. In contrast, in Fig. 3(b), we see that after collision three pulses emerge: an early, much weaker quasi-soliton (~ 24W), a later very high power quasi-soliton (~ 245W), and a final, very weak and dispersive wave (~ 0.002W) — the collision is highly inelastic. We note that this process is similar to what was described in Refs. [54, 55] for other NLSE variants. Systematically studying many such collisions, we find that the outcome can be modelled quite accurately using Eq. (5) which is similar as in a two-body resonance process. We emphasize that although the dispersive wave is fundamental for the energy transfer, its peak power is 5 orders of magnitude smaller than the solitons power, therefore negligible for the implementation of the effective model.

In Fig. 3(c), we show that agreement between Eq. (5) and the numerical simulations is indeed remarkably good. Indeed, Eq. (5) was used to generate the cascade model results for Figs. 1 and 2. We have further verified the accuracy of Eq. (5) by simulating a large number of individual collision processes with varying relative phases and varying initial quasi-soliton parameters. In Eq. (5), ϵ_{eff} is an empirical cross-section coefficient (see the appendix for an analytical justification assuming two-particle scattering). It depends on β_3 as shown in Fig. 3(d). The transition from a regime without RWs to a regime with well pronounced RWs appears rather abrupt. This indicates that already small, perhaps only local changes in β_3, and hence in the local composition of the optical fibre itself [28, 56], can lead to dramatic changes for the emergence of RWs. Indeed, we find that once a RW has established itself in the large-β_3 region, it continues to retain much of its amplitude when entering a $\beta_3 = 0$ region.

6. Calm before the storm

Looking more closely at the temporal vicinity of waves with particularly large power values, we find that these tend to be preceded by a time period of reduced power values. This "calm before the storm" phenomenon [19] can be observed in Fig. 4. In Fig. 4(a) we can clearly see an asymmetry in the normalized power $|u(\Delta t)|^2 / \langle |u(\Delta t)|^2 \rangle$ relative to the RW event at $\Delta t = 0$ ($\Delta t < 0$ denotes events before the RW). The average includes all RWs, defined here as large power events above a threshold of 150W (thresholds 200 and 300W show similar behaviour) and also two independent simulations of the gNLSE, both with parameters as in Fig. 2. The period of calm in power before the RW occurs lasts about $\Delta t = 1.5$ps at $z = 200$m. It broadens for larger distances, but an asymmetry is retained even at 500m. Physically, this effect can be understood as follows: a RW moves more slowly than the non-RW solitons. Upon interaction with a soliton, the RW gains in energy, but due to Eq. (3) and Eq. (4), slows down even more (cp. Fig. 2); the soliton, having overtaken the RW, has lost some of its energy, therefore leading to a reduction in intensity before the RW.

This finding is further supported by Fig. 4(b), where we note that the "calm before the storm", already observed for the gNLSE, is even clearer and more pronounced for the cascade model. We observe strong oscillations away from $\Delta t = 0$. These describe the simple quasi-soliton pulses which we used to model $u(t)$ in the cascade model. For the gNLSE, these oscillations are much less regular, although still visible. The time interval of the period of calm appears shorter in the cascade model while the amplitude reduction is stronger. We note that the apparently more regular oscillations in the cascade model at 200m is an artefact of our starting condition with solitons chosen perfectly equidistant at $z = 100$m to reproduce the same density as in the gNLSE.
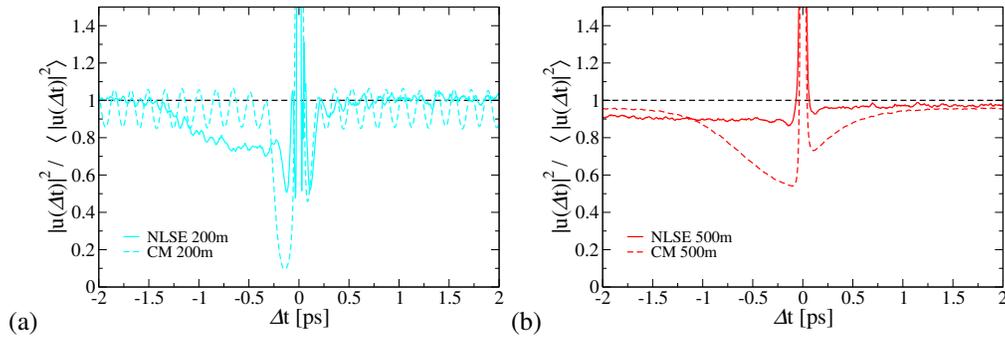
Fig. 4. Normalized averaged powers $|u(\Delta t)|^2 / \langle |u(\Delta t)|^2 \rangle$ for times Δt in the vicinity of a RW event at $\Delta t = 0$. Panel (a), (b) corresponds to 200 and 500m, respectively. Solid lines in both panels indicate averaged results for two gNLSE runs (with parameters as in Fig. 2), while dashed lines show the corresponding results for the cascade model. In both panels, we identify RWs as corresponding to powers equal to or larger than 150W. The colours are chosen to indicate distances compatible with a full set of results $z = 150, \ldots, 1500$m given in the appendix. Note that $|u(0)|^2 / \langle |u(0)|^2 \rangle > 10$ in both panels.

7. Methods

The numerical simulations of Eq. (1) were performed using the split-step Fourier method [47] in the co-moving frame of reference. A massively parallel implementation based on the discard-overlap/save method [60] was implemented to allow for simulations with 2^{31} intervals of $\Delta t = 1.8$fs and hence long time windows up to 3.865×10^6ps with several kilometres in propagation distance. We assume periodic boundary conditions in time and, as usual, a coordinate frame moving with the group velocity. The code scales linearly up to 98k cores.

We start the simulations with a continuous wave of $P_0 = 10$W power at $\lambda_0 = 1064$nm. For the fibre, we assume the parameters $\beta_2 = -2.6 \times 10^{-28} \text{s}^2\text{m}^{-1}$, $\gamma = 0.01 \text{ W}^{-1}\text{m}^{-1}$, and varying β_3 up to $1.7 \times (2.64 \times 10^{-42} \text{s}^3\text{m}^{-1})$, see Fig. 3. Due to the modulation instability, we observe, after seeding with a small 10^{-3}W Gaussian noise, a break-up into individual pulses within the first 100m of the simulation with a density of ~ 5.88 pulses/ps. Throughout the simulation, we check that the energy remains conserved. The PDF of $|u|^2$ is computed as the simulation progresses. For the two-quasi-soliton interaction study, we use the massively-parallel code as well as a simpler serial implementation. The collision runs are started using pulses of the quasi-soliton shapes (2) with added phase difference $\exp(i\phi)$ in the advanced pulse.

The effective cascade model assumes an initial condition of quasi-solitons of the same density of 5.88 quasi-solitons/ps. Their starting times are evenly distributed with separation $\Delta t \sim 0.17$ps while their initial powers are chosen to mimic the distribution observed in the gNLSE at $z \sim 100$m. The time resolution is 2×10^{-3}ps and we simulate the propagation in 1500 replicas of time windows of 4000ps duration. This gives an effective duration of 6×10^6ps. For all such 30×10^6 quasi-soliton pulses, we compute their speeds, find the distance at which the next two-quasi-soliton collision will occur and compute the quasi-soliton energy exchange via (5). The power of the emerging two pulses is calculated from $E_q = 2P_q T_q$ and the algorithm proceeds to find the next collision. The PDF of $|u|^2$ is computed assuming that the shape of each quasi-soliton is given by (2).

8. Conclusions

Our results emphasize the crucial role played by quasi-soliton interactions in the energy exchange underlying the formation of RWs via the proposed cascade mechanism. While interactions are

known to play an important role in RW generation [37–41, 43–45, 57, 58], the elucidation of the full cascade mechanism including its resonance-like quasi-soliton pair scattering and details such as the "calm before the storm", might be essential ingredients of any attempt at RW predictions. In addition, these features are quite different from linear focusing of wave superpositions [32, 33] and allow the experimental and observational distinction of both mechanisms.

RWs emerge when β_3 is large enough as shown in Fig. 3. Their appearance is very rapid in a short range $0.8 \lesssim \beta_3/2.64 \times 10^{-42}\text{s}^3\text{m}^{-1} \lesssim 1$. This can be understood as follows: the dispersion relation, in the moving frame, is $\beta(\omega) = \beta_2(\omega - \omega_0)^2/2 + \beta_3(\omega - \omega_0)^3/6$. The anomalous dispersion region of $\beta(\omega) < 0$, with soliton-like excitations, ends at $\omega_c - \omega_0 \geq -3\beta_2/\beta_3$ beyond which $\beta(\omega) \geq 0$ and dispersive waves emerge. From (3), we can estimate the spectral width as $2(\omega_c - \omega_0) = 2\pi\sqrt{\gamma P/|\beta_2|}$. This leads to the condition

$$\beta_3 \geq \frac{3|\beta_2|}{\pi}\sqrt{\frac{|\beta_2|}{\gamma P}} \approx 0.9 \times (2.64 \times 10^{-42})\text{s}^3\text{m}^{-1}, \tag{6}$$

which is in very good agreement with the numerical result of Fig. 3(c). In (6) the β_3 threshold that leads to fibres supporting RWs depends on the peak power P. In deriving the numerical estimate in (6) we have used a typical $P \sim 50\text{W}$ as appropriate after about $\sim 100\text{m}$ (cp. Fig. 1 and also the movies in [59]). Once such initial, and still relatively weak RWs have emerged, the condition (6) will remain fulfilled upon further increases in P due to quasi-soliton collisions, indicating the stability of large-peak-power RWs. Our estimation of the effective energy-transfer cross-section parameter ϵ_{eff} can of course be improved. However, we believe that Eq. (5) captures the essential aspects of the quasi-soliton collisions already very well. We find that simulations of Eq. (1) with $\beta_3 = 0$ but including an added Raman term [47] also affirm the essential role of quasi-soliton collisions [41] and are also well described by the cascade model [64]. Thus far, we have ignored fibre attenuation. Clearly, this would cause energy dissipation and eventually lead to a reduction in the growth of RWs and hence give rise to finite RW lifetimes. But as long as the fibre contains colliding quasi-solitons of enough power, RWs will still be generated.

Up to now, we have used the term RW only loosely to denote high-energy quasi-solitons as shown in Figs. 2 and 1. Indeed, a strict definition of a RW is still an open question and qualitative definitions such as *a pulse whose amplitude* (or energy or power) *is much higher than surrounding pulses* are common [28]. Our results now suggest, in agreement with recent work [28], a quantifiable operational definition at least for *normal* waves in optical fibres described by the gNLSE: a large amplitude wave is *not* a RW if it occurs as frequently as expected for the PDF at $\beta_3 = 0$ (cp. Fig. 1). We emphasise that both high spatial and temporal resolution are required to obtain reliable statistics for RWs in optical fibres for reliable predictions of the PDF. A small time window in the simulation can severely distort the tails of the PDF, and hence their correct interpretation.

We find that RWs are preceded by short periods of reduced wave amplitues. This "calm before the storm" has been observed previously [19] in ocean and in optical multifilament RWs, but not yet in studies of optical fibres. We remark that we first noticed the effect in our cascade model, before investigating it in the gNLSE as well. This highlights the usefulness of the cascade model for qualitatively new insights into RW dynamics. More results are needed to ascertain if the periods of calm can be used as reliable predictors for RW occurrence, i.e., reducing false positives. Last, we emphasise that the underlying cause for the RW emergence due to TOD or Raman terms is of course the absence of integrability. Our results suggest that, e.g., a suitable dispersion engineering for Eq. (1) even without TOD (or Raman term) could destabilize the solitons and lead eventually to the formation of RWs.
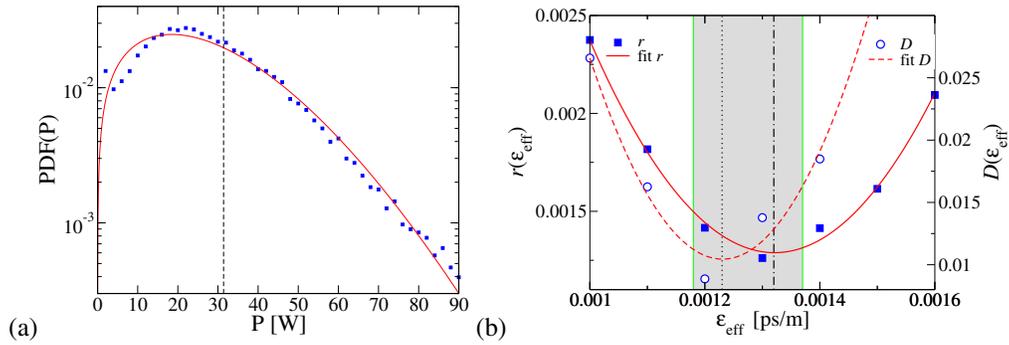
Fig. 5. (a) Normalized peak power distribution PDF(P) for $\beta_3 = 0$ at 1.5 km. The data points denotes (blue squares) denote the data while the solid (red) line shows the fit with Eq. (7). The dashed black line is at the fitted value $P_0 = 31.4$ W (b)Relative variance r (filled squares) and largest difference D (open circles) calculated for different values of ϵ_{eff} at $\beta_3 = 2.64 \times 10^{-42} \text{s}^3 \text{m}^{-1}$. Parabolic fits to the data are shown as lines. The vertical dotted line denotes the estimated $\epsilon_{\text{eff}} = (1.23 \pm 0.05)$fs/m at which D is minimal, the grey region indicates the error of that estimate. The vertical dashed-dotted line denotes the estimate $\epsilon_{\text{eff}} = (1.32 \pm 0.05)$fs/m from r.

A.   Further details of the cascade model

Choice of initial PDF

As initial condition for the cascade model we compute the PDF of the *soliton peak power*, P_q, in the NLSE case $\beta_3 = 0$. We select a distance of $z = 1500$m such that PDF($|u|^2$) has stabilized. We find that the resulting PDF(P_q) can be described as

$$\rho(P_q) = \frac{b}{P_0} \left(\frac{P_q}{P_0}\right)^{b-1} \exp\left[-\left(\frac{P_q}{P_0}\right)^b\right], \tag{7}$$

where $P_0 = 31.4 \pm 0.6$W and $b = 1.69 \pm 0.04$. The PDF(P_q) and its fit are shown in Fig. 5(a) (the fit has been performed taking the log of the data and the log of the fitting function). The value P_0 can alternatively be estimated using energy conservation. We start with a continuous wave (CW) power of $P_{\text{CW}} = 10$W. From the autocorrelation, we measure the average time between two peaks as $\Delta T = 0.170 \pm 0.008$ ps. Hence the initial energy contained in the time window ΔT is $E_{\text{init}} = P_{\text{CW}}\Delta T = 1.70$ pJ. At distances when quasi-solitons have been created the average energy contained in ΔT, using Eq. (3) and Eq. (7), is $E_{\text{final}} = \int_0^\infty 2P_q T_q(P_q)\rho(P_q)dP_q \simeq 1.796\sqrt{|\beta_2|P_0/\gamma}$. From energy conservation, $E_{\text{final}} = E_{\text{init}}$, we find $P_0 \simeq \gamma \left(P_{\text{CW}}\Delta T/1.796\right)^2 /|\beta_2| = 34 \pm 3$W.

Derivation of the effective quasi-soliton description

In section 2, we argued that the shape of a $\beta_3 \neq 0$ quasi-soliton can be approximated by Eq. (2). The argument follows Ref. [47]. The solution of Eq. (1) can be approximated as a soliton-like pulse

$$u(z,t) = \sqrt{P}\text{sech}\left[\frac{t-q(z)}{T}\right] \times \exp\left\{-i\Omega[t-q(z)] - iC\frac{[t-q(z)]^2}{2T^2}\right\}, \tag{8}$$

where P, T and C represent the amplitude, duration and chirp. The other two parameters are the temporal shift q of the pulse envelope and the frequency shift Ω of the pulse spectrum. The distance-dependence of the parameters can be obtained using the momentum method [47, 62, 63].

This gives

$$\frac{dT}{dz} = (\beta_2 + \beta_3\Omega)\frac{C}{T}, \qquad \frac{dC}{dz} = \left(\frac{4}{\pi^2} + C^2\right)\frac{(\beta_2 + \beta_3\Omega)}{T^2} + \frac{4\gamma P}{\pi^2},$$
$$\frac{dq}{dz} = \beta_2\Omega + \frac{\beta_3}{2}\Omega^2 + \frac{\beta_3}{6T^2}\left(1 + \frac{\pi^2}{4}C^2\right), \qquad \frac{d\Omega}{dz} = 0. \tag{9}$$

The equations can be solved for $C = 0$, resulting in Eq. (2) with $\phi = -\Omega(t - v^{-1}z)$, while T and v^{-1} have been given in Eq. (3) and Eq. (4).

B. Determining the energy gain

Deriving the energy gain formula

In Fig. 3 we observe an energy transfer due to inelastic scattering. This energy *gain* of quasi-soliton 1 from quasi-soliton 2, can be written as $\Delta E_1 = \int \mathcal{G}(P_1, \Omega_1, P_2, \Omega_2; z, t, \phi)dzdt$ [61], where $\mathcal{G}$ is an energy density and ϕ is the phase difference between the two quasi-solitons. It is convenient to change variables $s = t - z/v_1$, $w = t - z/v_2$. Such that

$$\Delta E_1 = \frac{1}{|v_1^{-1} - v_2^{-1}|}\int \mathcal{G}(P_1, \Omega_1, P_2, \Omega_2; s, w, \phi)\,dsdw. \tag{10}$$

Eq. (10) shows that a large difference between the (inverses of the) v_q results in a reduced energy gain for the larger quasi-soliton in agreement with the results in the main paper. Fourier-expanding Eq. (10), we can write

$$\frac{\Delta E_1}{E_2} = \frac{1}{|v_1^{-1} - v_2^{-1}|}\sum_{n=0}^{\infty}\epsilon_{P_1,\Omega_1,P_2,\Omega_2}(n)\cos\left[n(\phi - \phi_0)\right], \tag{11}$$

where $\epsilon(n)$ are Fourier coefficients (we suppress the P_q and Ω_q indices for a moment) and ϕ_0 is the phase difference for which the gain has a maximum. We approximate the above formula with just the first two coefficients. These two coefficients are related; indeed the larger quasi-soliton always gains energy ($\Delta E_1 > 0$), hence $\epsilon(0) \geq |\epsilon(1)|$ and because for a certain ϕ the energy gain is zero, we have $\epsilon(0) = -\epsilon(1)$. Thus we can write

$$\frac{\Delta E_1}{E_2} \simeq \frac{\epsilon_{P_1,\Omega_1,P_2,\Omega_2}}{|v_1^{-1} - v_2^{-1}|}\sin^2\left(\frac{\phi - \phi_o}{2}\right), \tag{12}$$

where we have used $1 - \cos(\phi) = 2\sin^2\left(\frac{\phi}{2}\right)$ and defined $\epsilon = 2\epsilon(0)$. The value of ϵ is yet undetermined while the dependence on the group velocities and the phase difference is clear. As shown in Fig. 3(c), Eq. (12) provides an excellent description of the energy gain in pair-wise quasi-soliton collisions. In order to determine the energy transfer we estimate the individual pulse energies in the gNLSE via $\int_{\Delta t}|u(z,t)|^2 dt$ with $\Delta t = 1$ps symmetric w.r.t. the maximum peak power. In the cascade model, we use $E_q = 2P_qT_q$. In principle, a collision can shift the soliton frequency $\Omega \to \Omega + \Delta\Omega$ and hence the dispersion via $\beta_2 + \beta_3\Delta\Omega$. The relative correction is $\sim (\beta_3/\beta_2)\Delta\Omega \propto 10^{-2}\Delta\Omega$ THz^{-1}. In the gNLSE simulations, we observe at most $\Delta\Omega \leq 3$THz, and the relative variation will be $\leq 3\%$. We thus ignore the effect and only consider the change in energy due to the peak power variation.

Effective coupling constant ϵ_{eff}

We want to model a system of many colliding quasi-solitons as shown in Fig. 2(a). The parameter $\epsilon_{P_1,\Omega_1,P_2,\Omega_2}$ depends on the individual power and frequency shift of each quasi-soliton pair. In

order to devise a tractable model, we have to find an effective ϵ_{eff} that describes the average properties of the u-amplitudes well. We therefore choose a distance $z = 500$, where from Fig. 2(a) we see that well-developed quasi-soliton pulses exist, while the situation is not yet RW dominated as shown in Fig. 1(a). We use a constant trial value for ϵ_{eff} and apply Eq. (5) to all quasi-soliton collisions in the cascade model computing data similar to Fig. 2(d) and Fig. 1(b). We repeat the calculation with another trial ϵ_{eff}. For different ϵ_{eff}, we compare the PDF created from the cascade model with the PDF obtained from the gNLSE and choose ϵ_{eff} such that the agreement is best (see below). We note that this process was followed for the ϵ_{eff} values shown in Fig. 3(d) for the different β_3 values. Furthermore, we have checked that similar results can be obtained by using $z = 300$ as the starting point of the analysis. Once ϵ_{eff} is determined, we use it to compute the results for the cascade model, starting at $z = 100$m and "propagating" all the way to 1500m as described in section 7. We emphasize the good agreement of the PDFs for $z \neq 500$m.

Estimating ϵ_{eff}

We are interested in determining ϵ_{eff} such that the PDFs of the gNLSE and the cascade model (CM) agree at $z = 500$m. Since we are interested in RWs we want that agreement to be good in the tail region of $|u|^2 > 150$W. We therefore define the relative variance

$$r(\epsilon_{\text{eff}}) = \frac{\sum_i \left[\log \text{PDF}_{\text{gNLSE}}(|u_i|^2) - \log \text{PDF}_{\text{CM}}(|u_i|^2, \epsilon_{\text{eff}})\right]^2}{\sum_i \left[\log \text{PDF}_{\text{gNLSE}}(|u_i|^2)\right]^2} \tag{13}$$

and minimize it with respect to ϵ_{eff} as shown in Fig. 5. The ϵ_{eff} at minimum is our estimate with accuracy $\epsilon_{\text{eff}}\sqrt{r(\epsilon_{\text{eff}})}$. The results for ϵ_{eff} calculated using this variance minimization are shown in Fig. 3(d) (red line).

As a second test, we perform a Kolmogorov-Smirnov (KS)-like two-sample test [60] between $\log \text{PDF}_{\text{gNLSE}}(|u_i|^2)$ and $\log \text{PDF}_{\text{CM}}(|u_i|^2, \epsilon_{\text{eff}})$. We need to renormalize the data count as $\widetilde{N}_i = \log(1 + N_i)$ with each j denoting a $|u_i|^2$ bin and overall $\widetilde{N} = \sum_{j=1}^{N_{\text{bins}}} \log(1 + N_i)$. Hence the effective number of data is given by $\widetilde{N}_e = (\widetilde{N}_{\text{gNLSE}}\widetilde{N}_{\text{CM}})/(\widetilde{N}_{\text{gNLSE}} + \widetilde{N}_{\text{CM}})$. Following the KS prescription, we then define the difference $D = \max_{i \in [1, N_{\text{bins}}]} \left|\text{CDF}_{\text{gNLSE}}(i) - \text{CDF}_{\text{CM}}(i)\right|$ and minimize it with respect to ϵ_{eff} as shown in Fig. 5 (b). As usual, with $\lambda = (\sqrt{\widetilde{N}_e} + 0.12 + 0.11/\sqrt{\widetilde{N}_e})D$, a KS-like accuracy can be given as $Q_{\text{KS}}(\lambda) = 2\sum_{j=1}^{\infty}(-1)^{j-1}e^{-2j^2\lambda^2}$, although it should no longer be interpreted probabilistically. The results for ϵ_{eff} calculated using this KS-like test are also shown in Fig. 3(d) with Q_{KS} given for each β_3 value. It is important to note that Q_{KS} remains roughly constant for all β_3 values, indicating a comparable level of similarity between PDF_{CM} and $\text{PDF}_{\text{gNLSE}}$ across the full β_3 range. In Fig. 5 (b), we show the ϵ_{eff} dependence of the test.

C. Fitting the PDFs

The PDFs of Fig. 1 have been fitted using the Weibull function

$$W(|u|^2) = ba^{-b}(|u|^2)^{b-1}\exp\left[-\left(\frac{|u|^2}{a}\right)^b\right] \tag{14}$$

The fits are shown in Fig. 1. Every fit has been performed taking the log of the $\text{PDF}(|u|^2)$ and $W(|u|^2)$, the resulting coefficients are in Table 1. Our results suggest that while a Weibull fit [19] is indeed possible for the tails, a systematic and consistent variation of the fitting parameters with distance travelled is not obvious. While, e.g., the PDF for 200, 500 and 1500m as shown in Fig. 1(a) appears sub-exponential in the tails, we find that the tail of the PDF for 1000m is

Table 1. Values of the coefficients a, b and F_0 needed to fit the various PDF($|u|^2$) distributions from Fig. 1 at three representative distances $z = 500$ m, 1000 m and 1500 m, using (W) the Weibull function of Eq. (14), (F) the stretched exponential of Eq. (15) and (P) the Pareto function as in Eq. (16). The reduced χ^2 value is also displayed.

Distance	Model	Fit	a	$b/10^{-1}$	$F_0/10^{-3}$	χ^2
500 m	gNLSE	W	4.0 ± 0.5	4.94 ± 0.15		1
		F	9 ± 21	6 ± 3	8 ± 30	50
		P	2.8 ± 0.2	150 ± 3		3700
	cascasde model	W	3.0 ± 0.5	4.60 ± 0.16		9
		F	12 ± 3	6.3 ± 3	6 ± 2	1060
		P	2.6 ± 0.2	130 ± 30		560
1000 m	gNLSE	W	0.9 ± 0.4	3.2 ± 0.2		4
		F	8 ± 10	47 ± 10	4 ± 5	136
		P	1.57 ± 0.15	55 ± 20		160
	cascasde model	W	0.7 ± 0.2	3.04 ± 0.14		11
		F	11 ± 5	4.9 ± 0.4	2 ± 1	3400
		P	1.51 ± 0.12	46 ± 15		660
1500 m	gNLSE	W	0.07 ± 0.03	2.1 ± 0.1		15
		F	0.006 ± 0.001	2.1 ± 0.4	50 ± 70	240
		P	1.00 ± 0.05	10 ± 2		64
	cascasde model	W	0.04 ± 0.01	1.94 ± 0.05		22
		F	0.008 ± 0.016	2.1 ± 0.3	120 ± 140	490
		P	0.87 ± 0.05	5.5 ± 1.6		6

super-exponential for $z \gtrsim 600$m. We also fitted the tails of PDF($|u|^2$) with a stretched exponential

$$F(|u|^2) = F_0 \exp\left[-\left(\frac{|u|^2}{a}\right)^b\right],\qquad(15)$$

and, following Ref. [40], with a Pareto function

$$Q(|u|^2) = \frac{ab^a}{|u|^{2(a+1)}}.\qquad(16)$$

The resulting coefficients are given in Table 1. For all fits, the results are not convincing as documented by the rather large χ^2 values found. This hints towards a continuing development of the shape of the PDF as the propagation continues.

Acknowledgments